CZECH TECHNICAL UNIVERSITY
IN PRAGUE

Faculty of Civil Engineering

Department of Mechanics

Bachelor's Thesis

Computational modeling of thermoset polymers with application to anchors

Jan Vozáb

Supervisor: Doc. Ing. Jan Vorel, Ph.D.

Prague, 2018

ČESKÉ VYSOKÉ UČENÍ TECHNICKÉ
V PRAZE

Fakulta stavebního inženýrství

Katedra mechaniky

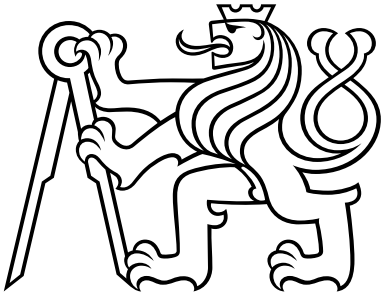

Bakalářská práce

Počítačové modelování reaktoplastů používaných v kotevních systémech

Jan Vozáb

Vedoucí práce: Doc. Ing. Jan Vorel, Ph.D.

Praha, 2018

ZADÁNÍ BAKALÁŘSKÉ PRÁCE

I. OSOBNÍ A STUDIJNÍ ÚDAJE

Příjmení: **Vozáb** Jméno: **Jan** Osobní číslo: **438389**

Fakulta/ústav: **Fakulta stavební**

Zadávající katedra/ústav: **Katedra mechaniky**

Studijní program: **Stavební inženýrství**

Studijní obor: **Konstrukce a dopravní stavby**

II. ÚDAJE K BAKALÁŘSKÉ PRÁCI

Název bakalářské práce:

Počítačové modelování reaktoplastů používaných v kotevních systémech

Název bakalářské práce anglicky:

Computational modeling of thermoset polymers with application to anchors

Pokyny pro vypracování:

Seznam doporučené literatury:

Jméno a pracoviště vedoucí(ho) bakalářské práce:

doc. Ing. Jan Vorel, Ph.D., katedra mechaniky FSv

Jméno a pracoviště druhé(ho) vedoucí(ho) nebo konzultanta(ky) bakalářské práce:

Datum zadání bakalářské práce: **19.02.2018** Termín odevzdání bakalářské práce: **27.05.2018**

Platnost zadání bakalářské práce: _____

doc. Ing. Jan Vorel, Ph.D. podpis vedoucí(ho) práce	podpis vedoucí(ho) ústavu/katedry	prof. Ing. Jiří Máca, CSc. podpis děkana(ky)

III. PŘEVZETÍ ZADÁNÍ

Student bere na vědomí, že je povinen vypracovat bakalářskou práci samostatně, bez cizí pomoci, s výjimkou poskytnutých konzultací. Seznam použité literatury, jiných pramenů a jmen konzultantů je třeba uvést v bakalářské práci.

. _____ _____

Datum převzetí zadání Podpis studenta

Prohlášení:

Prohlašuji, že jsem svou bakalárskou práci vypracoval samostatně a použil jsem pouze podklady (literaturu, projekty, software, atd.) uvedené v přiloženém seznamu.

Nemám závažný důvod proti užití tohoto školního díla ve smyslu § 60 Zákona č. 121/2000 Sb., o právu autorském, o právech souvisejících s právem autorským a o změně některých zákonů (autorský zákon).

V Praze dne

Jan Vozáb

Název práce:
Počítačové modelování reaktoplastů používaných v kotevních sytémech

Autor: Jan Vozáb

Obor: Konstrukce a dopravní stavby

Druh práce: Bakalářská práce

Vedoucí práce: doc. Ing. Jan Vorel, Ph.D.

Abstrakt:

Reaktoplasty mají v konstrukčním inženýrství důležitou roli. V porovnání s jinými odvětvími, jako je automobilový, letecký a kosmický průmysl, použité reaktoplasty nemusí být vždy v průběhu výstavby plně vytvrzené. Z tohoto důvodu může docházet ke změnám vlastností materiálu v důsledku dodatečného vytvrzování. Hlavním cílem této práce je vytvoření numerického modelu, který zachycuje dostatečně přesně vývoj materiálových vlastností a chování reaktoplastů při mechanickém zatěžování. Model v této práci je složen ze dvou částí. První je model vytvrzování, který zohledňuje vývoj materiálových parametrů v závislosti na teplotě a času. Jako druhý je použitý elasto-plastický model Drucker-Prager, který je využit na popis chování materiálu při mechanickém zatěžování.

Klíčová slova: dodatečné vytvrzování, reaktoplasty, Drucker-Prager, metoda konečných prvků

Title:

Computational modeling of thermoset polymers with application to anchors

Author: Jan Vozáb

Abstract:

Compared to their classical appearance in the aerospace or automotive industry, in civil engineering applications they typically do not reach a fully cured state during construction. Therefore, the material may undergo post-curing causing a significant change in material parameters. The main aim of this work is to create a numerical model that describes sufficiently precisely the evolution of material properties and the behavior of thermoset polymers during mechanical loading. The model in this thesis is composed of two parts. The first is a curing model that takes into account the development of material parameters in relation to temperature and time. The second is the elasto-plastic Drucker-Prager model, which is used to describe the behavior of the material during mechanical loading.

Key words: material curing, thermosetting polymers, Drucker-Prager, finite element method

Acknowledgment

I would like to say thank to my supervisor, Doc. Ing. Jan Vorel, Ph.D., for his time, patience and for incessantly explaining the same things to me all over again. I would like to thank to my friends and classmates for their support and continuous motivation. Great thanks also belong to my family and especially my girlfriend Radka Sochorová for their psychical support for the duration of making this thesis.

Contents

List of Figures

Introduction

In the last century construction engineering as well aerospace engineering were dominated by the materials steel, aluminum, and concrete. But especially in last decade civil engineers more than ever faced often contradictory demands for designing larger, safer and more durable structures at shorter time and lower costs. This lead to improvement of old and designing of new materials. Composites are a key element of those new designs.

Composite materials often combine positive characteristic properties from more, typically two, different materials which result to better material properties. In many cases these combine a load carrying constituent, typically in the form of carbon or glass fibers, bonded to the cement or polymer based matrices. Their applications can be found in transportation as well as in civil engineering fields. In the aerospace industry we can found entire structural members made of composite materials, but in the building industry the use of polymer-based composites is limited. A typical area are members applied to existing concrete or masonry such as adhesive anchors. The commonly used polymers, typically utilized, are exothermically reacting, thermosets, e.g. epoxies or vinyl-esters. They have high filler content (including even cement and water). They have uncertain curing level and the mechanical properties due to the environmental conditions (a fully cured state is not usually reached).

Also a large range of working temperatures, which are typically expected during the lifetime leads to a post-curing and related changes in mechanical properties. These changes highly impact, in particular, structures under sustained or cyclic loads. For these challenges, the characterization of this type of materials is in high demand.

The first chapter is focused on the description of anchors, the distribution according to the installation time and the load transfer mechanism, further failure modes of anchors are described. The second chapter is focused on thermosets, used types of polymers with anchors and overall material properties. In the third chapter models used for numerical simulation of thermoset polymers are introduced. As first of them, a non-associated Drucker-Prager model used for calculation of current stress and strain in time is explained. Then the curing model employed to calculate an evolution of material parameters is described. The fourth chapter is focused on the results and their comparison with experimental test data.

1 Anchor systems

An anchor is a steel element either cast into concrete or post-installed into a hardened concrete member and used to transmit applied loads, including headed bolts, hooked bolts (J- or L-bolt), headed studs, expansion anchors, or undercut anchors [1]. Anchors are typically used to connect structural elements or to fix non-structural components (or systems) to the structures.

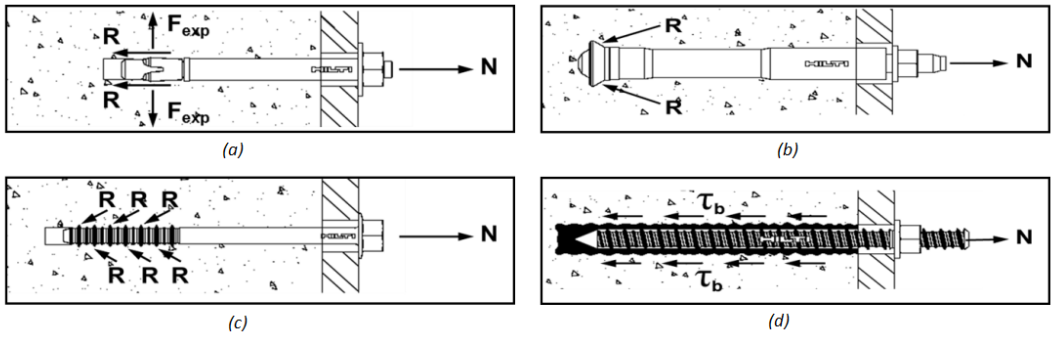

Figure 1.1: Types of post-installed anchors with different load transfer mechanism (R is direction of reaction force, N is loading of anchor and F_{exp} represent expansion force) [2]: a) friction (micro-keying); b) keying (bearing/undercut); c) keying (screw-type); d) adhesion (bonding).

1.1 Load transfer mechanisms

In the Fig. 1.1 we can see different types of load transfer mechanisms. The choice of a used mechanism affects future method of installation, resilience to different types of loading and even curing time, which some anchors need before loading. Each anchor type is described below in detail [2].

- *Friction mechanism:* As the name implies, the primary transfer mechanism is friction and it results in bonding from expansion forces between the anchor and the primary structure (Fig. 1.1a). Frictional force is proportional to the magnitude of expansion stresses generated by the anchor.The expansion is caused by a controlled torque during casting and even, in some cases, later adjusted for changes in the state of the base material.

- *Keying mechanism:* This transfer principle rely on the interlock of the anchor with deformations in the hole wall to resist external loading (Fig. 1.1b,c). The bearing stresses created in the base material in the interface with the anchor bearing surface

can rise to high values. This type of anchors offers good resilience to variations in the base material conditions and thus represent one of the most robust solutions for anchor designs.

- *Bonding mechanism:* This mechanism relies on adhesion between the concrete and the anchor created by adhesive (Fig. 1.1d). The degree of bonding available is depending on the conditions of the whole wall at the time of anchor installation and used type of adhesive material. This type of mechanism offers flexibility and high bond resistance for a wide variety of anchoring applications.

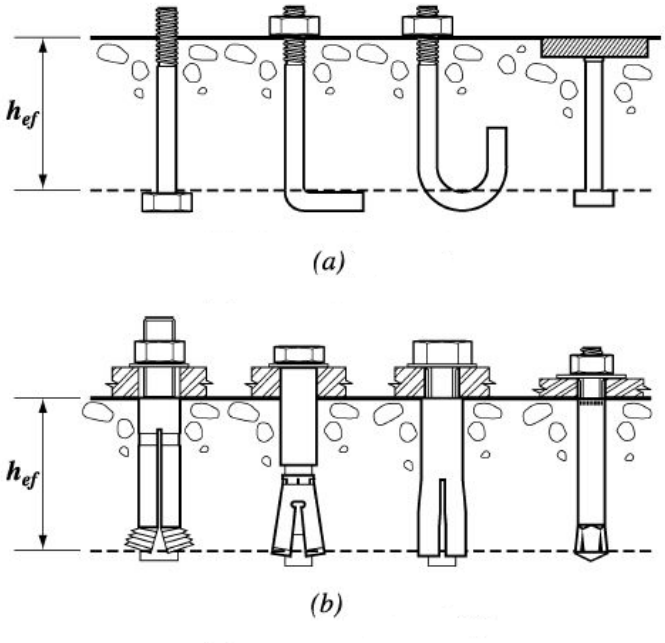

Figure 1.2: Types of anchors (h_{ef} is effective anchor length) [1]: a) cast-in-place; b) post-installed.

1.2 Types of anchors

Anchors can be divided by the load transfer mechanism, but another important criterion before choosing a specific solution is the installation time, when an anchor is fixed. As you can see in Fig. 1.2, anchors can be divided into two main groups: a) cast-in-place and b) post-installed.

1.2.1 Cast-in-place anchors

The cast-in-place anchors are the simplest type of anchor. As the name suggests, these anchors are cast in the wet concrete or with reinforcement of concrete. In the Fig. 1.2 we can see that designs can consist of a standard bolt with a hexagonal head (hex head bolt (a.1)), "hooked" J bolts (a.2) and L bolts (a.3). These anchors are very strong, and can be used in most anchor applications, butx they are also difficult to cast. Therefore, they are recommended when the large embedment length or the high tensile strength are required.

1.2.2 Post-installed anchors

Post-installed anchors are in general, technically sophisticated products, but are easy to install and provide more variability than cast-in anchors like headed studs. They can be cast into already hardened concrete as well as into masonry but they are a lot more sensitive to the boundary conditions than cast-in-place anchors. Most of the commercially available post-installed anchor products can be assigned to one of the major types which are categorized according to their load transfer mechanism (Fig. 1.1).

1.2.3 Types of post-installed anchors

Four main groups of post-installed anchors based on a load transfer mechanism and method of installation can be found in the literature [2].

- *Expansion anchors*, which have the primary principle of load transfer mechanism based on the friction, bearing or both. Anchors are inserted into a drilled hole in the hardened concrete or masonry. Main advantages are immediate load transfer and no temperature restrictions, but on the other hand they are not the best in transfer capacity.
- *Undercut anchors* create holding strength with the mechanical interlock provided by undercutting the concrete near the back of the hole. This is achieved by a special tool or by the anchor itself during installation. The main load transfer mechanism

is keying. This type of anchors have benefits like high transfer capacity, immediate loading transfer, or no temperature restrictions, but they are more difficult to install.

- *Screw anchors* are inserted into drilled hole with a diameter typically smaller than the anchor. Typical load transfer mechanism is keying. The advantages are immediate full loading transfer or no temperature restrictions, but the anchors can reach just low loading capacity.

- *Adhesive anchors* are post-installed into drilled hole in hardened concrete, masonry or stone. Loads are transferred to the base material by the bond created by an adhesive on the anchor, so the load transfer mechanism is a bonding. Advantages of this type of anchor are a simple installation and a high capacity. Main disadvantages are temperature restrictions and a curing time needed before loading. But full curing state is not typically reached. Modeling partly cured adhesive is difficult due to a large number of variables such a loading history, time, temperature, even humidity. Modeling of this adhesive material is the main target of this thesis.

1.3 Loading and failure modes

An anchor is in most cases loaded in tension and shear. This loading checks all parts of anchor, even the base material. According to a norm [1], the strength design of anchors shall be based either on computation using design modes that satisfy requirements of the norm, or on test evaluation using the 5 percent fractile of test results for the following:

- steel strength of anchor in tension,
- steel strength of anchor in shear,
- concrete breakout strength of anchor in tension,
- concrete breakout strength of anchor in shear,
- pullout strength of anchor in tension (including adhesive),
- concrete side-face blowout strength of anchor in tension,
- concrete pry out strength of anchor in shear.

These failure modes are shown in Fig. 1.3. However, adhesive anchors have even more complicated failure modes due to a full length bond, which can be damaged in different ways, see Fig. 1.4.

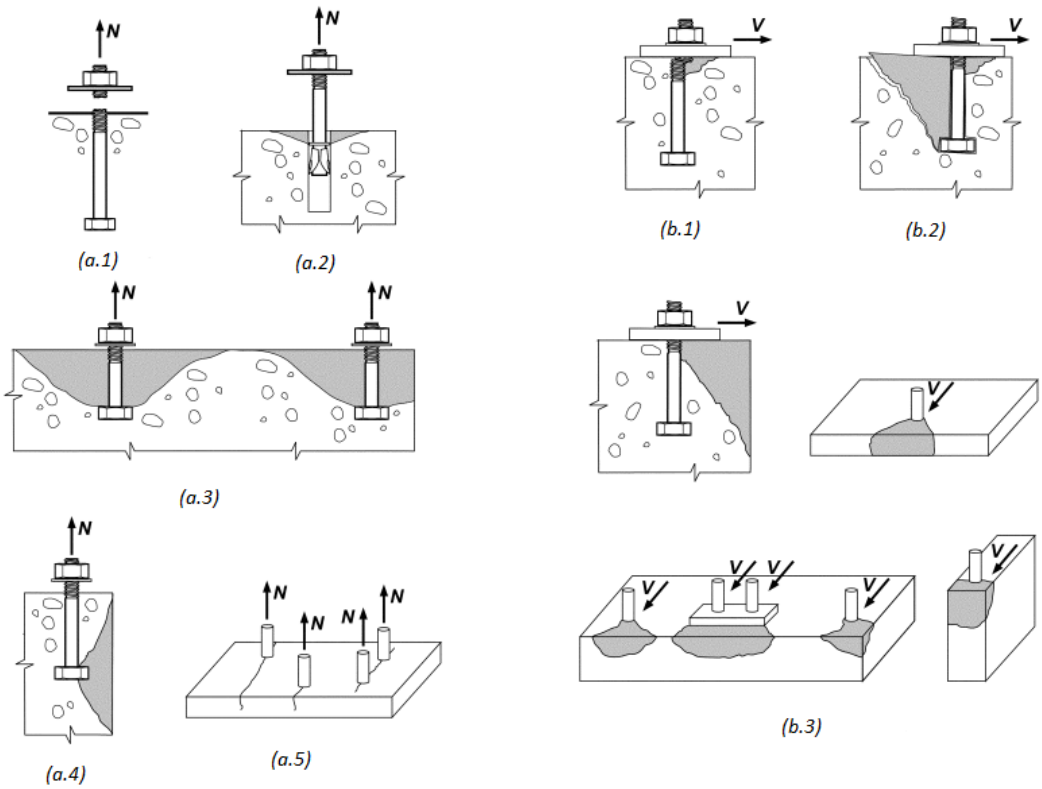

(a) tensile loading, where N is tensile force (b) shear loading, where V is shear force

Figure 1.3: Failure modes of anchors [1]: a.1) steel failure; a.2) pullout; a.3) concrete breakout; a.4) side-face blowout; a.5) concrete splitting; b.1) steel failure preceded by concrete spalling; b.2) concrete pryout for anchors far from a free edge; b.3) concrete breakout.

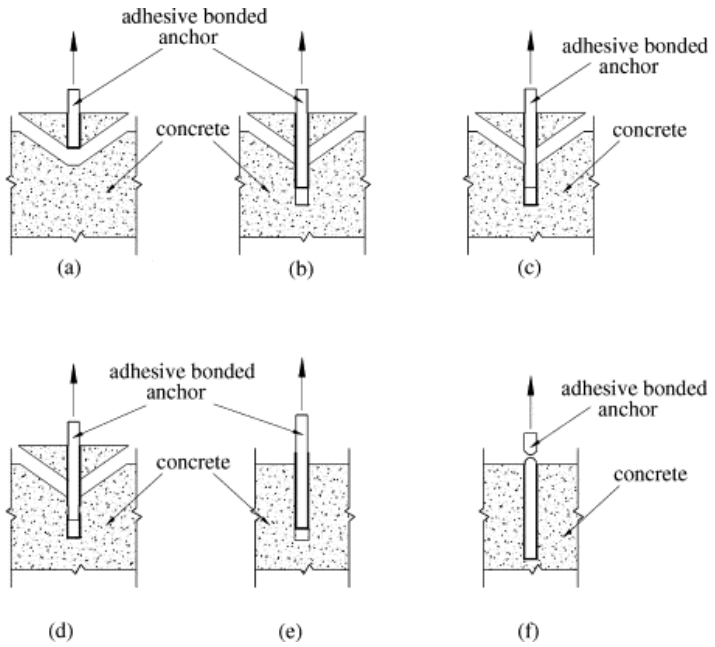

Figure 1.4: Failure modes of adhesive anchors in tension [3]: a) concrete cone failure; b) adhesive/concrete interface bond failure; c) steel/adhesive interface bond failure; d) mixed bond failure; e) bond failure; f) steel failure.

2 Thermoset polymers

Plastic materials may be classified into two main categories based on their response to temperature: thermoplastic and thermosetting polymers. A thermoplastic materials behaves like fluid above a certain temperature level, but the heating of a thermosetting material leads to its degradation without without transition to a fluid state. This classification is not restricted only to plastic materials but may also be extended to the behavior of coating, adhesives and several other categories. This is why we find it better to use the term *thermoset polymers*, which implies the different ways in which these materials are used and adds the fact that a constitutional repeating unit (CRU)[1] is present in their chemical structure. These materials are also referred to as *thermoset resins*, which is a vaguer definition that may be applied to the starting monomers or oligometric precursors, as well as to the final materials [4].

2.1 Thermoset polymers used with anchors

Utilized mortars, with reference to the anchor systems, are composed of thermoset polymers (e.g. vinyl-ester based and epoxy systems) and high filler content (e.g., sand, stone, cement) of about 40%.

2.1.1 Vinyl-ester systems

Vinyl-ester based system is a hybrid form of polyester resin which has been toughened with epoxy molecules within the main molecular structure and offers better resistance to moisture absorption, but it's downside is sensitivity to mixing, handling, atmospheric moisture and temperature sensitivity (sometimes it just will not cure). The toughening effect of the resin modifications makes a better resistance to micro fracturing and some of the secondary functionality of the backbone assisting in adhesion to substrates. Vinyl-esters are capable of forming secondary bonds around 3400 kPa. Vinyl-esters definitely represent an improvement over polyesters when considering standard peroxide curing, however adhesion to dissimilar and already cured substrates is still far below perfect and many vinyl-ester hulls suffer similar massive delamination of the hull skins from core and bulkhead substrates. It is also known that vinyl-ester resins bond very well to fiberglass, but offer a poor bond to kevlar and carbon fibers. Open surface curing vinyl-esters require a surfacing agent and subsequent applications require careful surface preparation if reasonable adhesion is to be achieved [4].

[1] The smallest constitutional unit which repetition constitutes a regular macromolecule, a regular oligomer molecule, a regular block or a regular chain.

2.1.2 Epoxy systems

Epoxy systems in all categories of work will realize the greatest degree of bond strength, water-resistance and toughness. Well-reinforced epoxy repair will tenaciously hold to the substrate with almost 14000 kPa strength. In areas that must be able to flex and strain with the fibers without micro-fracturing, epoxy resins offer much greater capability. Cured epoxy tends to be very resistant to moisture absorption. Epoxy resin will bond dissimilar or already-cured materials which makes repair work that is very reliable and strong. It actually bonds to all sorts of fibers very well and also offers excellent results in repair-ability when it is used to bond two different materials together. New generation of epoxy systems feature many of the advantages of low viscosity and accurately tailored gel and cure times [4].

2.2 Numerical description of thermoset polymers

In order to describe thermoset polymers, there are more degrees of complexity (in this thesis two), depending on the number of variables taken into account in constitutive equations under consideration (see also [4]).

- *First level*, where these equations could take into account only two variables: the stress σ and the strain ε:

$$f(\sigma, \varepsilon) = 0. \tag{2.1}$$

This limits model mechanical simulation for relatively sharp intervals of time and temperature. It can be considered sufficient for a description of material behavior at low strains. For the isotropic material, moduli are defined by the following equations:

$$E = 3K(1-2\nu); \quad G = \frac{3}{2}\frac{(1-2\nu)}{(1+\nu)}; \quad K = \frac{E}{2(1+\nu)}, \tag{2.2}$$

where E is the elastic (Young) modulus, G means the shear (Coulomb) modulus, K represent the bulk modulus, and ν is Poisson's ratio. E can be obtained from a uniaxial tensile test ($E = \sigma/\varepsilon$), or a uniaxial compressive test, or flexural test; G can be determined from a shear test $G = s/\gamma$, where s is the shear stress and γ is the shear strain; K can be determined from a compressibility test,

$$K = \left(\frac{1}{V}\frac{dV}{dp}\right)^{-1}, \tag{2.3}$$

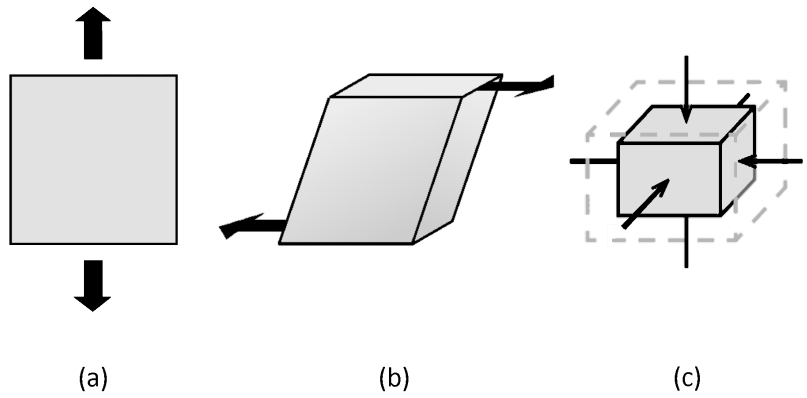

Figure 2.1: Mechanical tests used for determination a) E; b) G; c) K.

where V is the volume and p is the hydrostatic pressure; and ν can be figured out from two independently determined values of modulus, or from a tensile test using a bidimensional extensometer.

- *Second level*, where the constitutive equations must involve two (or more) additional variables. For instance:

$$f(\sigma, \varepsilon, \dot{\varepsilon}, T, t, c, \Theta) = 0, \tag{2.4}$$

where $\dot{\varepsilon}$ is the strain rate, T means the temperature, t represents time , c is the moisture content and Θ stands for the mechanical dilatation. These new variables are necessary for, e.g., addition of viscoelastic behavior into the material model. This behavior is linked to the molecular motions, which are important in the glassy domain (in the Fig. 2.2 between boundaries α and β). Also they affect the behavior in the glass transition region (around boundary α). High influence on the behavior also have thermo-mechanical history due to an anchor installation and a physical aging of the material. The relationships that describe the effects of $\dot{\varepsilon}$, $\dot{\sigma}$, T, t, c and Θ on the previously defined elastic properties are also needed if the extensive model is adopted.

  In the literature we can find three major experimental methods for mechanical characterization in this region, which correspond to particular solutions of the material's state equation:

  - Static tests: $\varepsilon = \varepsilon_0 = constant$ for relaxation, or $\sigma = \sigma_0 = constant$ for creep.
  - Monotonous tests with loading rate $\dot{\varepsilon}$, or $\dot{\sigma} = constant$ (for example tensile tests):

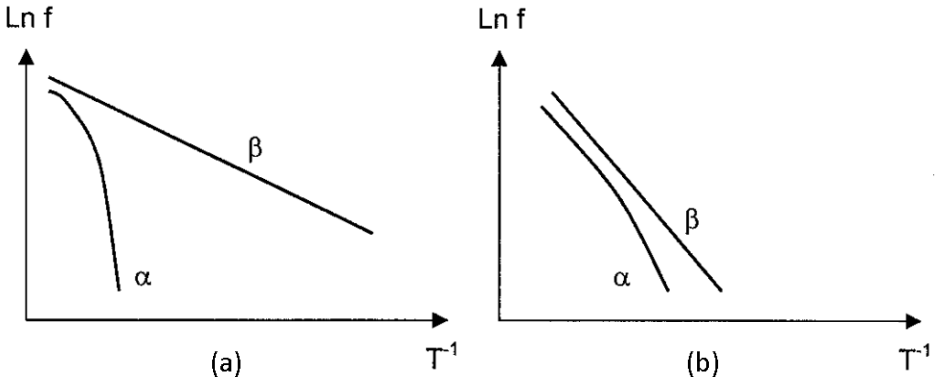

Figure 2.2: Shape of relaxation maps: dependence of $\ln f$ (frequency) to reciprocal temperature for coordinates of transitions α, β: (a) - polymers having their α and β transitions well separated; (b) - polymers with close α and β transitions

$$\dot{\varepsilon} = \frac{1}{l}\frac{dl}{dt}$$

– dynamic tests: $\varepsilon = \varepsilon_0 \sin(\omega t)$, or $\sigma = \sigma_0 \sin(\omega t)$

Polymers are generally assumed to obey the Boltzmann superposition principle in the region of small strains. When there are changes of loading conditions, the effects of these changes are additive when the corresponding responses are considered at equivalent times. For example, if different stresses σ_0, σ_1, σ_2,...σ_i are applied at different times 0, t_1, t_2,...t_i, respectively, the final strain is

$$\varepsilon(t) = J(t)\sigma_0 + J(t-t_1)\sigma_1 + J(t-t_2)\sigma_2 + \cdots + J(t-t_i)\sigma_i \tag{2.5}$$

where $J(t)$ is the time-dependent creep compliance.

In the same manner, if different strains ε_0, ε_1, ε_2,...ε_i are applied at times 0, t_1, t_2,...t_i, the final stress is

$$\sigma(t) = E(t)\varepsilon_0 + E(t-t_1)\varepsilon_1 + E(t-t_2)\varepsilon_2 + \cdots + E(t-t_i)\varepsilon_i \tag{2.6}$$

where $E(t)$ is the time-dependent relaxation modulus. It is generally effective to use dynamic tests to obtain $J(\omega)$ or $E(\omega)$, and then with using mathematical transformations determine $J(t)$ or $E(t)$.

Ordinary, polymers obey a time-temperature superposition principle:

$$P_r(t,T) = P_r\left(\frac{t}{a_T}, T_r\right) \tag{2.7}$$

where P_r is function of T_r and a_T. In Eq. (2.7), T_r is a reference temperature and a_T is a thermal shift factor that depend on temperature, humidity and mechanical dilatation. Polymers are interesting in that $a_T = f(T, c, \Theta)$ takes different mathematical forms below and above glass transition temperature T_g.

2.3 Material properties

Material properties, needed for studying model performance of thermoset polymers, are directly connected to degree of complexity which is being investigated. As you can see in Sec. 2.2, in the first level basic mechanical properties are needed, e.g. Young's modulus E and Poisson's ratio ν. But such low number of material properties makes model limited to relatively sharp intervals of time and temperature, and functioning at low strains.

A higher level of complexity is needed to capture the complicated material behavior. This leads to the more specific material properties, which include yielding and fracture properties, volumetric properties, cohesive properties, glass transition properties, crosslink density, chain mobility, viscoelastic properties, curing degree and aging of the material, see also [4]. Some of them are described below in a more detail.

- Yielding properties define boundary between reversible and permanent deformation, but also behavior of the material over this boundary. In normal conditions, the material must be used below the yield boundary, often called the elastic limit of material. If the stress goes beyond its yield boundary, the ultimate fracture stress (lost of material integrity) becomes important. Then we need specific theoretical and experimental tools, e.g. fracture mechanics, to study these phenomena.

- Volumetric properties include free volume, density, packing density and expansion. Free volume is an intrinsic property of the polymer matrix and is created by the gaps left between entangled polymer chains. It can affect absorption and diffusion of the molecules in polymers.

- Cohesive properties are represented by the cohesive energy as the whole energy of intermolecular interactions, which is easy to determine from calorimetric measurements[1], and cohesive energy density.

- Glass transition is a catastrophic softening of the material, when temperature is higher then the glass transition temperature T_g. Also has influence to the curing process due to its exothermal behavior.

[1] For small molecules

- Viscoelastic properties include creep and relaxation properties, which describe connections between the stresses and strains with respect to time. Creep means increasing of the strains in time with constant stress and relaxation means reduction of the stresses under constant strains.
- Curing degree defines change of the material from the liquid to the glassy state. Note that bonded anchors have an uncertain curing degree of the mortar when they are loaded.

3 Computational modeling

For modeling of thermoset polymers we have used three methods of numerical solution. Firstly, the Drucker-Prager plasticity model used to simulate the mechanical behavior. The implementation follows the approach presented in [5]. More specifically, the robust object-oriented finite element (FE) solver MARS [6] is utilized for the implementation. Therefore, the curing model for polymers already implemented in MARS can be later utilize to account for the evolving of material properties caused by the change of curing degree.

3.1 Finite element method

Finite element method (FEM) is a numerical solution used for the simulation of stresses, strains, natural frequency, heat transition, electromagnetic effects, flow of fluids, etc., on a created physical model. The main principle is the discretization of continuum into finite number of elements. FEM is typically used to simulate the realistic behavior of structures or for determination of critical regions of structures. Through principles of this method were developed in first half of twentieths century, its massive expansion occurred with succession of a modern computer technologies due to necessary high computing power. The detail of description of FEM is out of the scope of this thesis and can be found in [7].

3.2 Drucker-prager model of plasticity

Drucker-Prager (DP) model of plasticity can be seen as the extension of the von Mises model and enhances it by including mean stress into the yield surface equation. Unlike Mohr-Coulomb (MC) model, the Drucker-Prager yield criterion is smooth and in space of the principal stresses have form of cylindrical cone, see Fig. 3.2. In current implementation parameters are adjusted to fit or inscribe to Mohr-Coulomb model. The main advantage of DP over MC is the simplification of return to the yield surface because of its smoothness. As already mentioned, the definition and the calculation of Drucker-Prager model in this thesis is based on [5].

3.2.1 Drucker-Prager yield surface

Drucker-Prager yield criterion equation describes boundary, where material ceases to behave elastically and becomes elasto-plastic and can be written as

$$F(\sigma) = J + (\sigma_m - c(\kappa_1)\cot\varphi(\kappa_2))M_{JP}(\varphi(\kappa_2)) = 0, \tag{3.1}$$

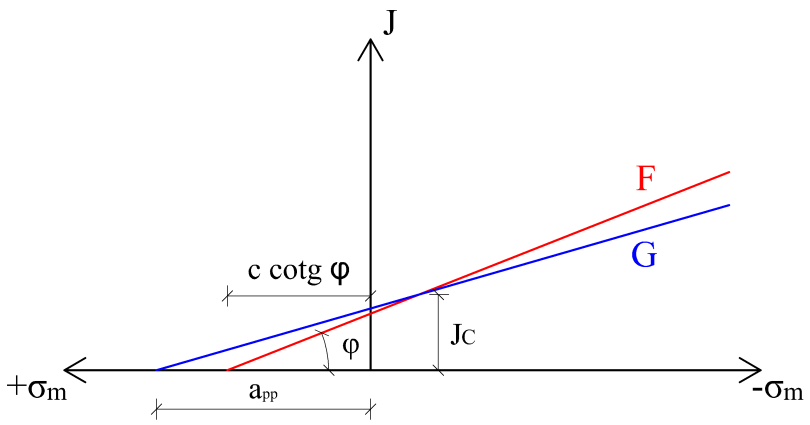

Figure 3.1: Drucker-Prager yield criterion in meridian plane [5]: F is yield function; G means plastic potential function.

where J is a square root of the second invariant of the deviatoric stress, σ_m is the mean stress with the form

$$J = \sqrt{\frac{1}{6}\left[(\sigma_{11}-\sigma_{22})^2 + (\sigma_{11}-\sigma_{33})^2 + (\sigma_{22}-\sigma_{33})^2\right] + \tau_{12}^2 + \tau_{13}^2 + \tau_{23}^2}, \tag{3.2}$$

$$\sigma_m = \frac{\sigma_{11}+\sigma_{22}+\sigma_{33}}{3}, \tag{3.3}$$

and M_{JP} is used for approximation to the Mohr-Coulomb model, which can be done with more forms dependent on point, which is intended to approximate. Three different Drucker-Prager cones are in the Fig 3.2. The first one, red circle, touches Mohr-Coulomb yield criterion at $\theta = 30°$ (triaxial compression) with M_{JP} defined as

$$M_{JP}^{\theta=30°} = \frac{2\sqrt{3}\sin\varphi}{3-\sin\varphi}, \tag{3.4}$$

where φ is the angle of internal friction. The second, blue circle, match the Mohr-Coulomb model at $\theta = -30°$ (triaxial tension), can be obtained as

$$M_{JP}^{\theta=-30°} = \frac{2\sqrt{3}\sin\varphi}{3+\sin\varphi}, \tag{3.5}$$

and the last, the green circle, is inscribed, and can be determined by

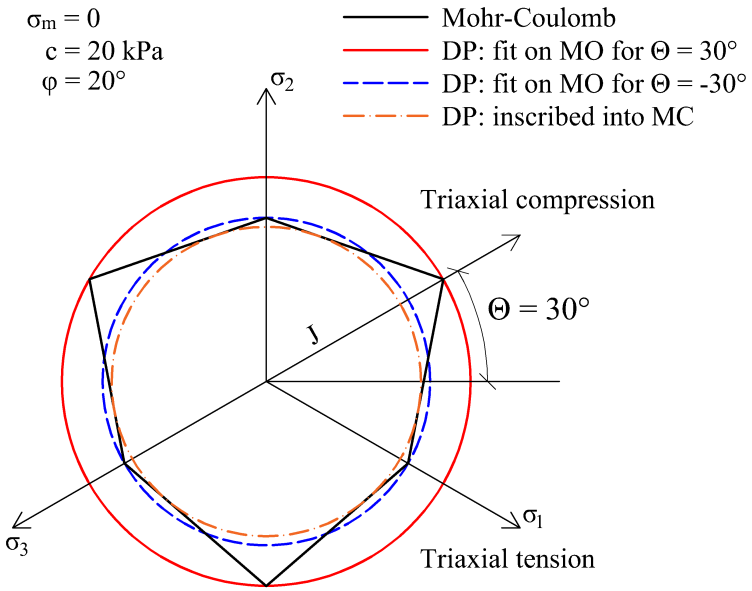

Figure 3.2: Drucker-Prager and Mohr-Coulomb yield criterion in space of principal stresses [5].

$$M_{JP}^{ins} = \frac{\sin(\varphi)}{\cos(\theta)^{ins} - \frac{\sin(\theta^{ins})\sin(\varphi)}{\sqrt{3}}}, \tag{3.6}$$

$$\theta^{ins} = \arctan\frac{\sin\varphi}{\sqrt{3}}. \tag{3.7}$$

The Drucker-Prager model is not defined just by the yield function F but also G, which is the plastic potential function, see Fig. 3.1. G defines vector of return to the yield of plasticity, when it is overpassed, and can be written in the form

$$G = J + [\sigma_m - a_{pp}]\, M_{JP}^{PP} = 0, \tag{3.8}$$

where a_{pp} follows from Fig. 3.1. When matching Eqs. (3.1) and (3.8) for the current value of stress σ, result has the form

$$a_{pp} = -\sigma_m^c + (\sigma_m^c - c\cot\varphi)\frac{M_{JP}}{M_{JP}^{PP}} \tag{3.9}$$

By substituting a_{pp} into the plastic potential function (3.8), we arrive at

$$G = J + \left[\sigma_m - -\sigma_m^c + (\sigma_m^c - c\cot\varphi)\frac{M_{JP}}{M_{JP}^{PP}}\right] M_{JP}^{PP} = 0, \tag{3.10}$$

where M_{JP}^{PP} is the gradient of the plastic potential function in $J - \sigma_m$ space (Fig 3.1).

When functions of plastic potential and yield function $M_{JP}^{PP} = M_{JP}$, Drucker-Prager model becomes associated. M_{JP}^{PP} can be referred as the angle of dilatation ψ, and can be substituted for φ in Equations (3.4)-(3.7).

3.2.2 Hardening and softening modulus

In Drucker-Prager model implemented derivation of hardening/softening modulus is inspired by the von Mises. To that end, we choose multi-linear form of the hardening/softening law for the cohesion c and the angle of internal friction φ, as shown in Fig. 3.3, where the dependence of c and φ on the deviatoric plastic strain E_d^{pl} can be seen. Though the components of vector κ may vary for each of the two strength parameters, in the present formulation a single hardening parameter is assumed

$$\kappa = \kappa_1 = \kappa_2 = E_d^{pl}. \tag{3.11}$$

Multi-linear formulation assumes that if n^{th} interval in the Fig. 3.3 is active, then the current strenght parameters can be determined by

$$c = c^{n-1} + h_c^n \left(E_d^{pl} - (E_d^{pl})^{n-1} \right), \tag{3.12}$$

$$\varphi = \varphi^{n-1} + h_\varphi^n \left(E_d^{pl} - (E_d^{pl})^{n-1} \right), \tag{3.13}$$

where h_c^n and h_φ^n are the hardening/softening moduli for c and φ and can be written in the form

$$h_c^n = \frac{c^n - c^{n-1}}{(E_d^{pl})^n - (E_d^{pl})^{n-1}} \tag{3.14}$$

$$\varphi_c^n = \frac{\varphi^n - \varphi^{n-1}}{(E_d^{pl})^n - (E_d^{pl})^{n-1}} \tag{3.15}$$

Following [5], the hardening modulus can be determined by

$$H = \left(-\frac{\partial F}{\partial \kappa} \right)^T \frac{\partial \kappa}{\partial \lambda}, \tag{3.16}$$

and referring to Fig. 3.3 and using Eq. (3.16) the hardening/softening modulus H assumes the form

$$H = -\frac{\partial F}{\partial c} \frac{\mathrm{d}c}{\mathrm{d}E_d^{pl}} \frac{\mathrm{d}E_d^{pl}}{\mathrm{d}\lambda} - \frac{\partial F}{\partial \varphi} \frac{\mathrm{d}\varphi}{\mathrm{d}E_d^{pl}} \frac{\mathrm{d}E_d^{pl}}{\mathrm{d}\lambda}, \tag{3.17}$$

where

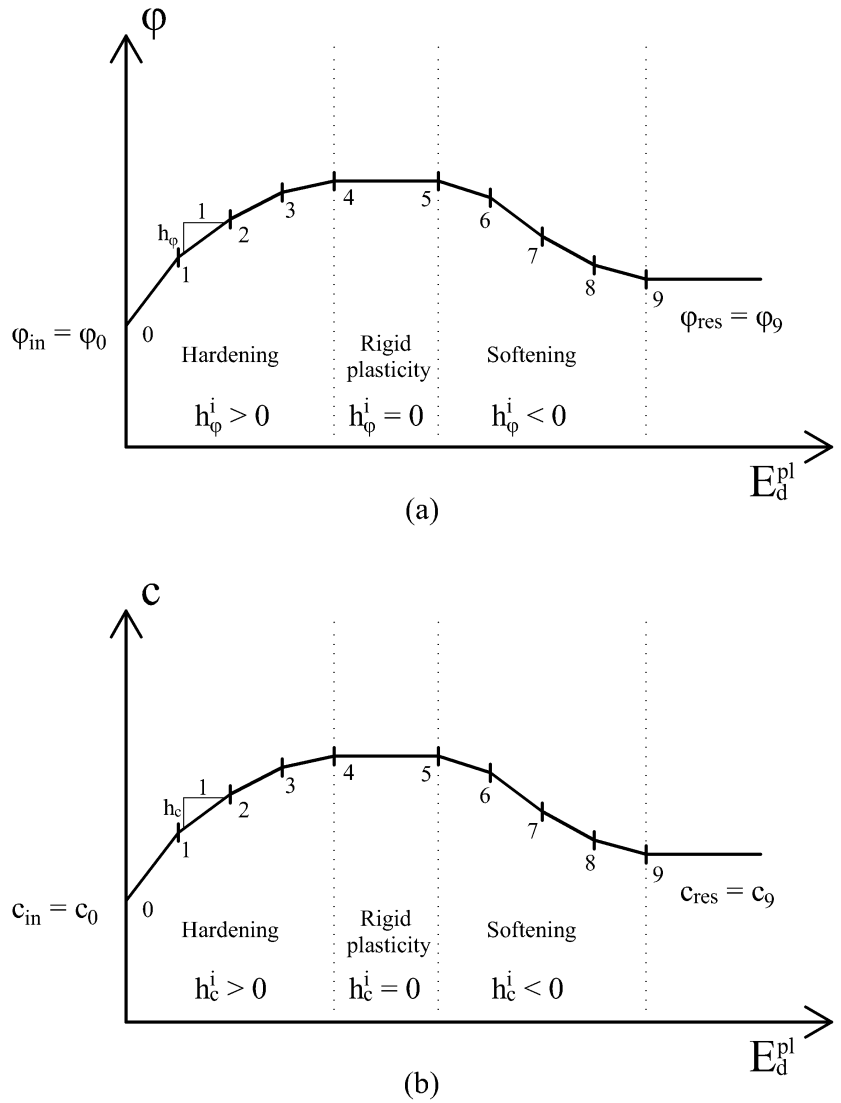

Figure 3.3: Hardening and softening modulus [5]: c_{in} and c_{res}, respective φ_{in} and φ_{res} represent initial and residual values of c and φ.

$$\frac{\partial F}{\partial \varphi} = \frac{c}{\sin^2 \varphi} M_{JP} + (\sigma_m - c \cot \varphi) \frac{\mathrm{d}M_{JP}}{\mathrm{d}\varphi}, \tag{3.18}$$

$$\frac{\mathrm{d}F}{\mathrm{d}c} = -\cot \varphi M_{JP}, \tag{3.19}$$

$$\frac{\mathrm{d}c}{\mathrm{d}\kappa} = \frac{\mathrm{d}c}{\mathrm{d}E_d^{pl}} = h_c, \tag{3.20}$$

$$\frac{\mathrm{d}\varphi}{\mathrm{d}\kappa} = \frac{\mathrm{d}\varphi}{\mathrm{d}E_d^{pl}} = h_\varphi \tag{3.21}$$

Derivations of M_{JP} with respect to φ for selected values of θ are

$$\frac{\mathrm{d}M_{JP}^{ins}}{\mathrm{d}\varphi} = \frac{3\sqrt{3}\cos\varphi}{(3+\sin^2\varphi)^{\frac{3}{2}}}, \tag{3.22}$$

$$\frac{\mathrm{d}M_{JP}^{\theta=-30^\circ}}{\mathrm{d}\varphi} = \frac{6\sqrt{3}\cos\varphi}{(1-\sin\varphi)^2}, \tag{3.23}$$

$$\frac{\mathrm{d}M_{JP}^{\theta=30^\circ}}{\mathrm{d}\varphi} = \frac{6\sqrt{3}\cos\varphi}{(1+\sin\varphi)^2}. \tag{3.24}$$

By accepting the strain hardening approach, we can write

$$\mathrm{d}\kappa = \mathrm{d}E_d^{pl} = \sqrt{2(\Delta e^{pl})^T \Delta e^{pl}} = \mathrm{d}\lambda \Rightarrow \frac{\mathrm{d}E_d^{pl}}{\mathrm{d}\lambda} = 1, \tag{3.25}$$

where Δe^{pl} stands for the increment of deviatoric plastic strain vector. With final substitution of Eq. (3.18)-(3.25) back into Eq. (3.17), result is searched form of the hardening/softening modulus as

$$H = h_c \cot\varphi M_{JP} - h_\varphi \left[\frac{c}{\sin^2\varphi} M_{JP} + (\sigma_m - c\cot\varphi)\frac{\mathrm{d}M_{JP}}{\mathrm{d}\varphi}\right]. \tag{3.26}$$

3.2.3 Calculation procedure and implementation

Total stress can be calculated as

$$\sigma = \mathbf{D}^{el}\varepsilon_{el}, \tag{3.27}$$

where $\mathbf{D}^{el}$ is an ordinary isotropic stiffness matrix and ε_{el} is a elastic deformation. Calculation is performed in explicit software [6], so model is implemented in the incremental form. Then Eq. 3.27 is modified as

$$\sigma^{n+1} = \sigma^n + \mathbf{D}^{el}\mathrm{d}\varepsilon_{el}. \tag{3.28}$$

During numerical procedure, the trial stress $\sigma_{tr}^{n+1} = \sigma^n + \mathbf{D}^{el}\mathrm{d}\varepsilon$, where $\mathrm{d}\varepsilon$ is a strain increment, is calculated at the beginning of each step. If Eq. (3.1) is satisfied, strains and stresses are stored, and calculation continues with next deformation increment. If the yield function is violated, the material behavior changes from the basic elastic to the elasto-plastic with hardening. Due to higher amount of the variables, which describe return to the yield surface of plasticity, is necessary to implement the Jacobian matrix[1]. There are four material parameters driving the return to yield surface of plasticity:

[1]Matrix of partial derivations

- $\Delta\lambda$ - Coefficient of plastic flow,
- c - Cohesion,
- φ - Angle of friction,
- ψ - Angle of dilatation.

Before describing the Jacobian matrix, we need to define basic equations, to be used for the definition of all variables. Assume that the plastic strain increment have the form

$$\mathrm{d}\varepsilon^{pl} = \Delta\lambda \frac{\partial G}{\partial \sigma}, \tag{3.29}$$

and with accepting this flow rule, increments of yield respective plastic strain have the form

$$\mathrm{d}\varepsilon_{\nu}^{pl} = \mathrm{d}\lambda \frac{\partial G}{\partial \sigma_m} = \Delta\lambda M_{JP}^{PP} \sin\psi, \tag{3.30}$$

$$\mathrm{d}E_{d}^{pl} = \mathrm{d}\lambda \frac{\partial G}{\partial J} = \Delta\lambda, \tag{3.31}$$

which further allows writing the corresponding stresses at the end of the $i+1$ load increment as

$$\sigma_m^{i+1} = \sigma_m^{tr} - K M_{JP}^{PP} (\sin\psi^{i+1}) \Delta\lambda, \tag{3.32}$$

$$J^{i+1} = J^{tr} + \mu\Delta\lambda, \tag{3.33}$$

where K is the bulk modulus and μ represent the elastic shear modulus to avoid misinterpretation with the plastic potential function. Then the Jacobian matrix can be already defined.

- Primary variables

$$\{\mathbf{a}\}^T = \{\Delta\lambda, c^{i+1}, \varphi^{i+1}, \psi^{i+1}\}. \tag{3.34}$$

- Residuals

$$\{\mathbf{r}\}^T = \{\mathcal{F}, \mathcal{C}, \Phi, \Psi\}, \tag{3.35}$$

where

$$\mathcal{F} = \overbrace{J^{tr} - \mu\Delta\lambda}^{J^{i+1}} + [\overbrace{\sigma_m^{tr} - KM_{JP}^{PP}(\sin\psi^{i+1})\Delta\lambda}^{\sigma_m^{i+1}} - c^{i+1}\cot\varphi^{i+1}]M_{JP}(\sin\varphi^{i+1}), \quad (3.36)$$

$$\mathcal{C} = c^{i+1} - \hat{c} = 0, \quad (3.37)$$

$$\Phi = \varphi^{i+1} - \hat{\varphi} = 0, \quad (3.38)$$

$$\Psi = \psi^{i+1} - \hat{\psi} = 0. \quad (3.39)$$

Variables $\hat{c}$ and $\hat{\varphi}$ follows Eq.(3.12) and (3.13) and the current value of dilatation angle $\hat{\psi}$ can be, with help of Rowe's dilatation theory in triaxial compression, written as

$$\sin\hat{\psi} = \frac{\sin\varphi^{i+1} - \sin\varphi_{cv}}{1 - \sin\varphi^{i+1}\sin\varphi_{cv}}, \quad (3.40)$$

where φ_{cv} is a constant-volume friction angle.

- Local Newton-Raphson method

$$\{a^{i+1}\}_{k+1} = \{a_k^{i+1}\} - [\mathbf{H}]^{-1}\{r\}_k \quad (3.41)$$

- Jacobian matrix $[\mathbf{H}]$

$$[\mathbf{H}] = \begin{bmatrix} \frac{\partial J}{\partial\Delta\lambda}\frac{\partial\mathcal{F}}{\partial\sigma_m}\frac{\partial\sigma_m}{\partial\Delta\lambda} & \frac{\partial\mathcal{F}}{\partial c} & \frac{\partial\mathcal{F}}{\partial\varphi} + \frac{\partial\mathcal{F}}{\partial M_{JP}}\frac{\partial M_{JP}}{\partial\sin\varphi} & \frac{\partial\mathcal{F}}{\partial M_{JP}^{PP}}\frac{\partial M_{JP}^{PP}}{\partial\sin\psi} \\ \frac{\partial\mathcal{C}}{\partial\hat{c}}\frac{\partial\hat{c}}{\partial\Delta\lambda} & \frac{\partial\mathcal{C}}{\partial c} & 0 & 0 \\ \frac{\partial\Phi}{\partial\sin\hat{\varphi}}\frac{\partial\hat{\varphi}}{\partial\Delta\lambda} & 0 & \frac{\partial\Phi}{\partial\sin\varphi} & 0 \\ 0 & 0 & \frac{\partial\Psi}{\partial\sin\hat{\psi}}\frac{\partial\sin\hat{\psi}}{\partial\sin\varphi} & \frac{\partial\Psi}{\partial\sin\psi} \end{bmatrix} \quad (3.42)$$

where partial derivations are

$$\frac{\partial J}{\partial \Delta\lambda}\frac{\partial \mathcal{F}}{\partial \sigma_m}\frac{\partial \sigma_m}{\partial \Delta\lambda} = -\mu - KM_{JP}^{PP}M_{JP}, \tag{3.43}$$

$$\frac{\partial \mathcal{F}}{\partial c} = -M_{JP}\tan\varphi, \tag{3.44}$$

$$\frac{\partial \mathcal{F}}{\partial \varphi} + \frac{\partial \mathcal{F}}{\partial M_{JP}}\frac{\partial M_{JP}}{\partial \sin\varphi} = M_{JP}\frac{c}{\sin^2\varphi\cos\varphi} + \left(\sigma_m\frac{c}{\tan\varphi}\right)\frac{\mathrm{d}M_{JP}}{\mathrm{d}\sin\varphi}, \tag{3.45}$$

$$\frac{\partial \mathcal{F}}{\partial M_{JP}^{PP}}\frac{\partial M_{JP}^{PP}}{\partial \sin\psi} = -K\Delta\lambda\frac{\mathrm{d}M_{JP}^{PP}}{\mathrm{d}\sin\psi}, \tag{3.46}$$

$$\frac{\partial \mathcal{C}}{\partial \hat{c}}\frac{\partial \hat{c}}{\partial \Delta\lambda} = -h_c, \tag{3.47}$$

$$\frac{\partial \mathcal{C}}{\partial c} = 1, \tag{3.48}$$

$$\frac{\partial \Phi}{\partial \sin\hat{\varphi}}\frac{\partial \hat{\varphi}}{\partial \Delta\lambda} = -\cos(\varphi)h_\varphi, \tag{3.49}$$

$$\frac{\partial \Phi}{\partial \sin\varphi} = 1, \tag{3.50}$$

$$\frac{\partial \Psi}{\partial \sin\hat{\psi}}\frac{\partial \sin\hat{\psi}}{\partial \sin\varphi} = -\frac{1-\sin^2\varphi_{cv}}{1-\sin\varphi\sin\varphi_{cv}}, \tag{3.51}$$

$$\frac{\partial \Psi}{\partial \sin\psi} = 1. \tag{3.52}$$

Derivation of M_{JP} with respect to $\sin\varphi$ is not written in exact form due to variable equation of M_{JP} (3.4)-(3.6).

- Initial conditions

$$\{a_0\}^T = \{0, c^i, \sin\varphi^i, \sin\psi^i\}, \tag{3.53}$$

$$\{r_0\}^T = \{J^{tr} + (\sigma_m^{tr} - c^i\cot\varphi^i)M_{JP}(\sin\varphi^i), 0, 0, 0\}. \tag{3.54}$$

3.2.4 Apex problem

Two cones are shown in Fig. 3.4. First cone K_ε (following direction of the plastic strain vector), shows inadmissible region for the plastic strain increment. Second cone K_σ shows the admissible stress domain. If the stress point is located in a region K_σ, material behavior is elastic, if it is located outside of K_σ but also outside of K_ε, the computation performs regular stress return. However, if the stress point is located inside the K_ε cone, the stress update is simply a return mapping to the apex. That situation may occur in two cases: (a) right after load increment, but also (b) when performing regular stress

return, due change of material parameters. Such a situation can be called as an "apex problem".

$$\dot{\varepsilon}_v \geq M_{JP}^{PP} \dot{E}_d^{pl}. \tag{3.55}$$

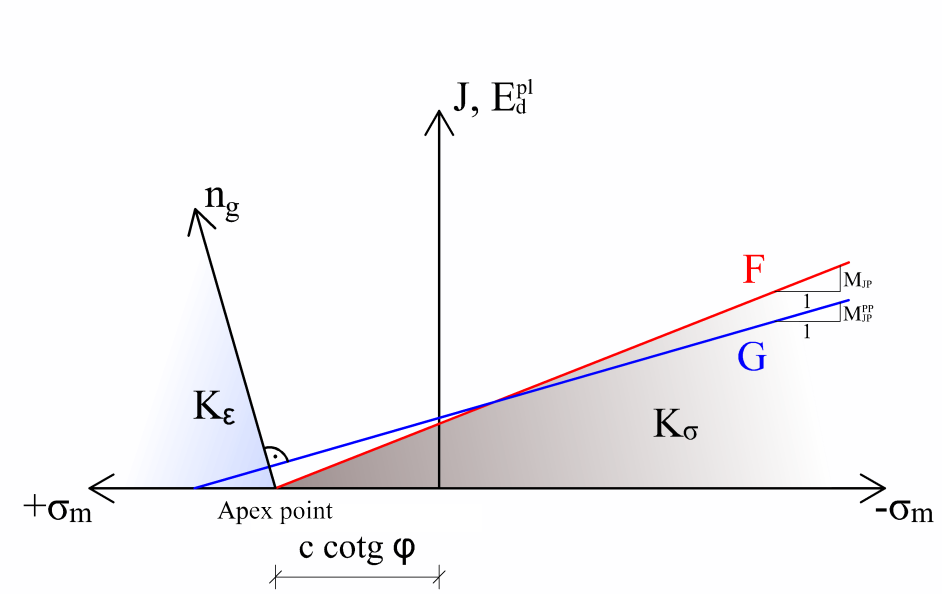

Figure 3.4: Apex admissible regions for stresses and plastic strain rates [5].

In the literature we can find two different stands for performing apex problem:

- Return with constant material parameters.
- Return with hardening/softening material.

At the first case, stress point just return to the apex (Fig.3.4), so stress takes the form

$$\sigma^{i+1} = 3c^i \cot \varphi^i \mathbf{m}. \tag{3.56}$$

If the second approach is chosen, we can use two facts. The first is that material parameters c and φ are functions of E_d^{pl}. The second is that when returning to the apex point, elastic strain have only volumetric part so ΔE_d^{pl} can be determined at first, because it does not change. And if elastic strain have only volumetric part, deviatoric plastic strain vector is equal to the deviatoric increment strain vector. Then $\mathrm{d}E_d^{pl}$ can be determined by the deviatoric strain measure, which has the form

$$\Delta E_d^{pl} = \sqrt{2 \Delta e_{ij}^{pl} \Delta e_{ij}^{pl}} \tag{3.57}$$

where e^{pl} represent deviatoric plastic strain vector. As next, hardening of parameters c and φ follows Eqs. (3.12) and (3.13) with current E_d^{pl}. Then the stress takes the form with updated c and φ, similar to Eq. (3.56), as

$$\sigma^{i+1} = 3c^{i+1} \cot \varphi^{i+1} \mathbf{m}. \tag{3.58}$$

3.3 Curing model

Behavior of thermoset polymers is difficult to simulate due to a large number of variables. Instead of making one complex model we decided to achieve more realistic behavior of our model with two simpler models. First is for the mechanical response, as you can se above. The second is a curing model based on [8], which is already implemented in MARS solver [6] and thus is utilized in the proposed approach based on the serial coupling of the models.

This model simulates generation of heat during the curing of polymers. The curing of an epoxy is in fact exothermic chemical reaction, and degree of cure is often measured by placing small element into a digital scanning calorimeter, which is maintaining the sample at constant temperature and measures generated heat during the curing. The degree of cure is often defined by

$$\phi(t) = \frac{H(t)}{H_r}, \tag{3.59}$$

where H_r represent the total heat generated. That means $\phi(t)$ increases from 0 to 1 at fully cured state. Rate of heat generation per unit mass have the form

$$r = \frac{\mathrm{d}(H_r \phi)}{\mathrm{d}t}. \tag{3.60}$$

The curing process is defined by a kinetic equation

$$\frac{\mathrm{d}\phi}{\mathrm{d}t} = f(T, \phi) \tag{3.61}$$

where T represents temperature and $f(T, \phi) \geq 0$ is represented by

$$d(T, \phi) = (k_1(T) + k_2(T()\phi^m)(1 - \phi)^n, \tag{3.62}$$

$$k_1(T) = A_1 \exp\left(-\frac{\Delta E_1}{TR}\right), \tag{3.63}$$

$$k_2(T) = A_2 \exp\left(-\frac{\Delta E_2}{TR}\right), \tag{3.64}$$

where m and n are constants, R means the gas constant, A_1, respective A_2, are frequency like constants and ΔE_1, respective ΔE_2, represent activation energies. For more information about these constants see also [8]. When the structural composite is cured, process of heat generation due to curing is affected by heat conduction due to the presence of an external surface or along fibers. This process can be described by the local form of the first law of thermodynamics as

$$\rho \frac{\mathrm{d}\epsilon}{\mathrm{d}t} = -\frac{\partial q_i}{\partial \chi_i} + \rho r + \sigma_{ij} \frac{\mathrm{d}}{\mathrm{d}t} \varepsilon_{ij}, \tag{3.65}$$

where ϵ it the internal energy per unit mass, ρ represent the current mass density, q_i are the components of the heat flux vector, r means the heat supply per unit mass, σ_{ij} are the stress components and ε_{ij} are the components of the infinitesimal strain tensor. The rate of mechanical work $\sigma_{ij} \frac{\mathrm{d}\varepsilon_{ij}}{\mathrm{d}t}$, is assumed to be negligible and the internal energy is assumed to be proportional to temperature, $e = cT$, where c is the specific heat capacity. The heat flux vector is related to the temperature gradient by the Fourier law of heat conduction with the form

$$q_i = -\kappa \frac{\partial T}{\partial \chi_i}, \tag{3.66}$$

where κ is the thermal conductivity. It is possible that the thermal conductivity depends on the degree of cure and the temperature $\kappa = \kappa(T, \phi)$. The Eq. (3.65) with (3.61) and (3.66) and the started assumptions becomes

$$\rho c \frac{\partial T}{\partial t} = \frac{\partial}{\partial \chi_i} \left(\kappa(T, \phi) \frac{\partial T}{\partial \chi_i} \right) + \rho H_r \frac{\partial \phi}{\partial t}. \tag{3.67}$$

Eqs. (3.61), (3.62) and (3.67) are a system of coupled nonlinear partial differential equations for the partial distribution and time variation of temperature and degree of cure based on the energy consideration.

If the degree of cure is calculated, we can determine the evolution of the longitudinal modulus $M(\phi)$, the shear modulus $\mu(\phi)$ and the bulk modulus $K(\phi)$. According to [8] the evolution of these parameters can be written as:

$$\mu(\phi) = \frac{1}{2} \frac{\beta_\mu (\mu_f - \mu_s)}{\left(1 + (\phi - 1/2)^2 \beta_\mu^2\right) \arctan(1/2\beta_\mu))}, \tag{3.68}$$

$$M(\phi) = \frac{1}{2} \frac{\beta_M (M_f - M_s)}{(1 + (\phi - 1/2)^2 \beta_M^2) \arctan(1/2\beta_M))} + K_{liq}, \tag{3.69}$$

$$K(\phi) = M(\phi) - \frac{4}{3} \mu(\phi), \tag{3.70}$$

where β_μ and β_M are fitting constants, μ_s, μ_f, M_s and M_f are the start and final value of

the measure shear and longitudinal moduli. The bulk modulus of the liquid epoxy have the form

$$K_{liq} = K_{tot}(0) = M_{tot}(0), \tag{3.71}$$

where total moduli can be determined by an analytical functions:

$$\mu_{tot} = \frac{\arctan\left((\phi - \frac{1}{2})\beta_\mu\right)}{\arctan\left(\frac{\beta_\mu}{2}\right)}(\mu_f - \mu_s) + \left(\frac{\mu_f + \mu_s}{2}\right), \tag{3.72}$$

$$M_{tot} = \frac{\arctan\left((\phi - \frac{1}{2})\beta_M\right)}{\arctan\left(\frac{\beta_M}{2}\right)}(M_f - M_s) + \left(\frac{M_f + M_s}{2}\right). \tag{3.73}$$

3.4 Complex material model

For the simulation of thermosetting polymers and their response we choose the approach with two serially coupled models. The aforementioned curing model is employed to calculate the evolution of material properties utilized by the Drucker-Prager model. This model uses the modified material parameters and calculates current stress and strain in a current time.. This would affect model behavior and, hopefully, provide more realistic results than a simple Drucker-Prager model. Note that this thesis represents a preliminary study and it is expected that more complex mechanical model, e.g. Microplane M4, will be utilized to characterize the mechanical behavior in more details. However, only results without the coupling are shown hereafter to verify the proper implementation of involved material models.

4 Results

To verify the model implementation of both aforementioned models in MARS solver [6], the numerically obtained data are compared to experimental measurements [8, 9] and corresponding conclusions are drawn.

4.1 Testing of Drucker-Prager model

To verify the proper implementation and to check the ability of Drucker-Prager model to capture the behavior of thermoset polymers, the simple compression test of hybrid vinyl-ester mortar presented in [9] is utilized. The test setup and specimen dimensions are shown in Fig. 4.1. The material properties of this material presented also in [9] at 25°C are: $E = 6792$ MPa; $\nu = 0.3$. Moreover, the parameters used for simulations using the Mohr-Coulomb yield criterion with an associated flow-rule in [9] are: $\phi = 28^{\circ}$ and $c = 26.1$ MPa. As can be seen in Fig. 4.2, linear 3D 8-node fine elements with 8 integration points are employed to discretize the specimen. To mimic the real setup, two rigid bodies (plates) are used to apply the load. The bottom plate is fixed in all directions and the rotation is not allowed, the top plate is fixed in horizontal directions and can rotate about horizontal axes. The load is applied by means of the prescribed displacement of the top plate in the vertical direction. The sliding with friction constraint is used for the contact between the specimen and plates, see [6] for more details. The general deformation of the specimen in the plastic regime is also presented in Fig. 4.2.

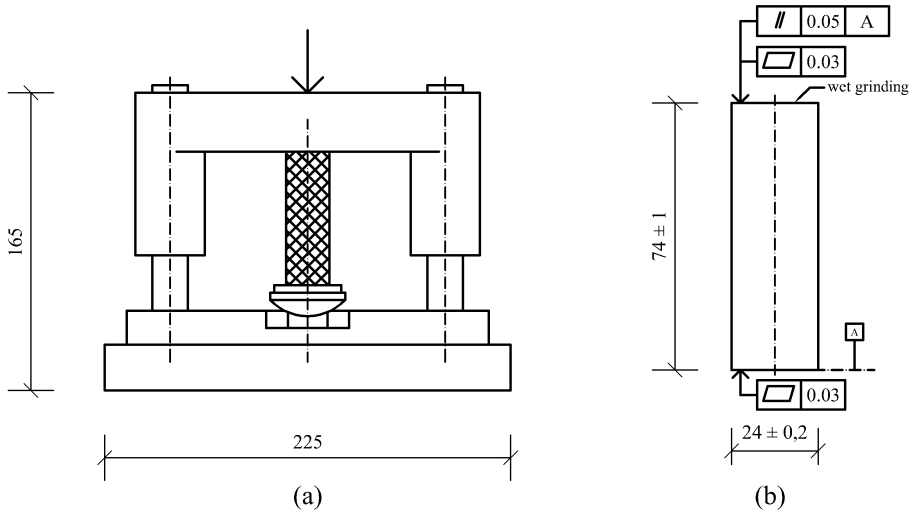

Figure 4.1: Compression test parameters [9]: a) setup; b) specimen dimensions.

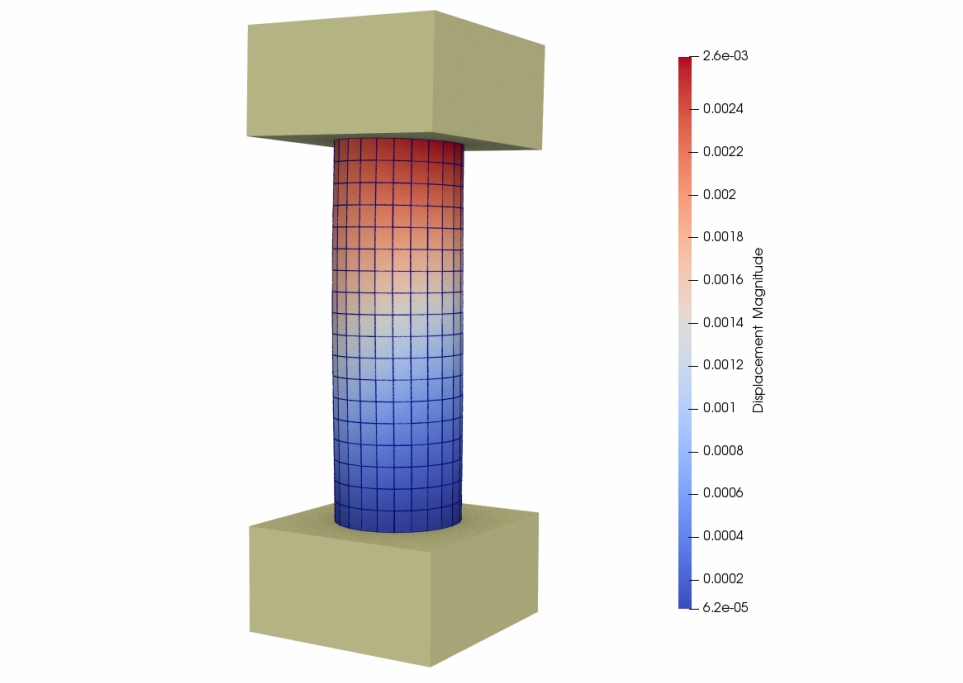

Figure 4.2: Compression test sample: on the surface you can see computed magnitude of displacement of the Drucker-Prager model without hardening of parameters.

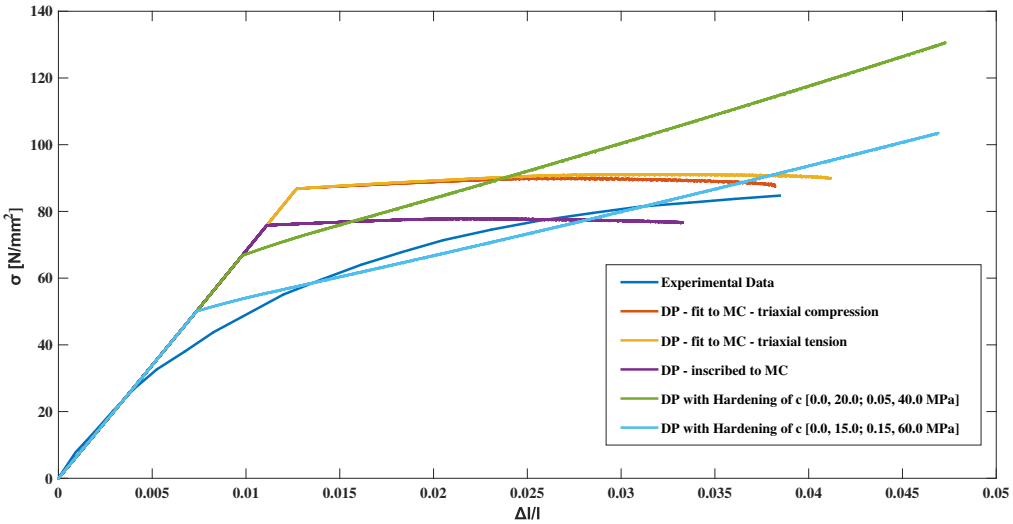

Figure 4.3: Compression tests compared to the real specimen result [9]

The numerical results, obtained for different material parameters, are compared to the experimental data [9] in Fig. 4.3. The red line stands for the Drucker-Prager model, where M_{JP} is computed according to Eq. (3.4), the orange line represents the use of Eq. (3.5) and the purple line corresponds to M_{JP} calculated according to Eq. (3.6). All

these simulations assume the parameters presented above, the associated flow-rule is also employed, i.e. $\psi = \phi$. The remaining simulations assume the evolution of cohesion with respect to E_d^{pl} (hardening). The response for the evolution defined by $c = 20$MPa for $E_d^{pl} = 0$ and $c = 40$MPa for $E_d^{pl} = 0.05$ is represented by the green line in Fig. 4.3. The updated evolution characterized by $c = 15$MPa for $E_d^{pl} = 0$ and $c = 60$MPa for $E_d^{pl} = 0.15$ is utilized to match the experimental data (light blue line). As can be seen, if the hardening is assumed, the numerical simulation adequately matches the experimental data. However, it has to be mentioned that the final conclusions cannot be drawn yet since only one loading scenario is utilized. To properly characterize the model suitability for studied thermoset polymers, additional experimental data are needed. As mentioned in [9], the extension of Drucker-Prager model by Rankine failure criterion or compressive cap.

Figs. 4.4 – 4.6 show the distribution of model parameters, internal model variables and strains for the relative elongation $\Delta L/L = \ldots$ of the material model with the hardening ($c = 15\,\text{MPa}$ for $E_d^{pl} = 0$ and $c = 60\,\text{MPa}$ for $E_d^{pl} = 0.15$). Fig. 4.4 clearly demonstrate the prescribe constant value of friction angle, distribution of deviatoric plastic strain measure and corresponding cohesion. The plastic and total strain components with respect to global coordinate system (z-axis is the axis of symmetry) are shown in Figs. 4.5 and 4.6, respectively.

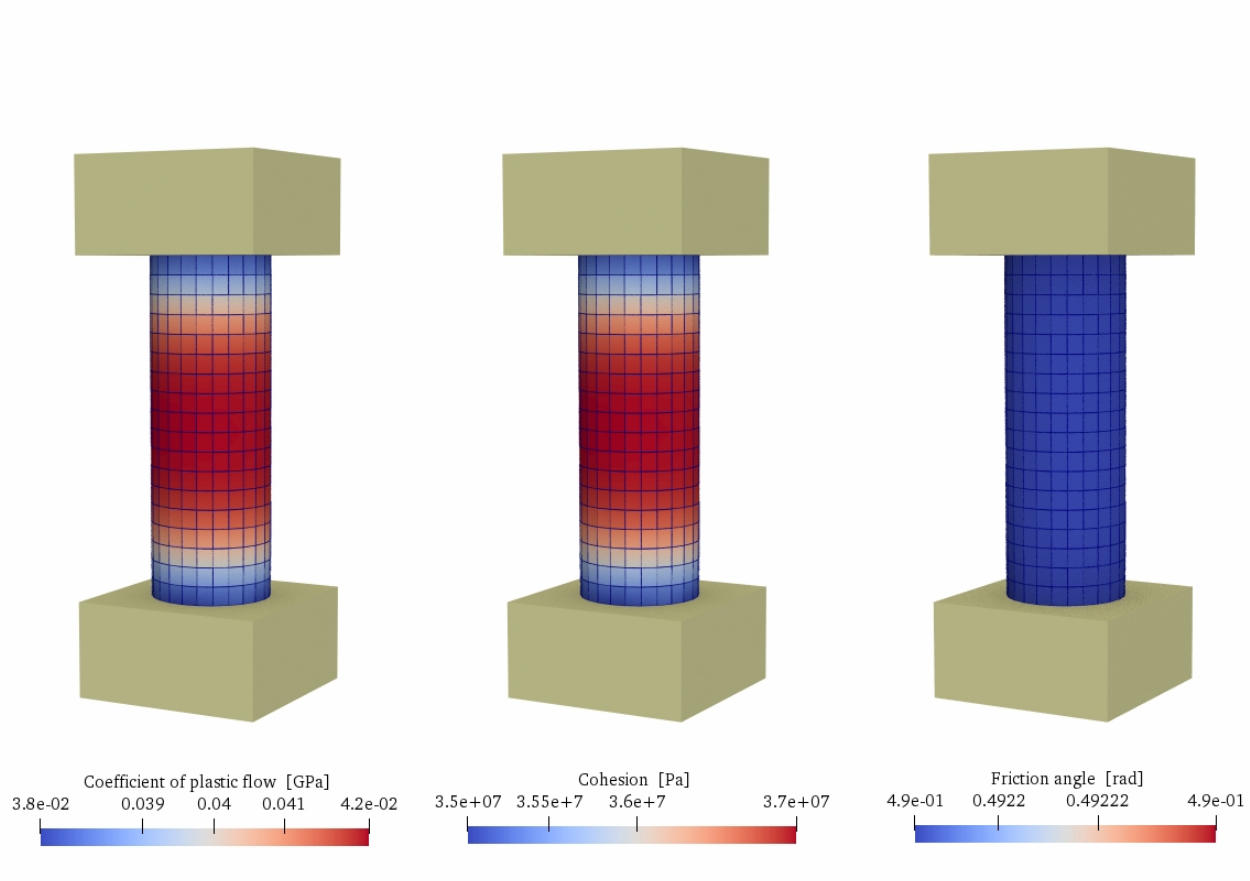

Figure 4.4: Distribution of model parameters.

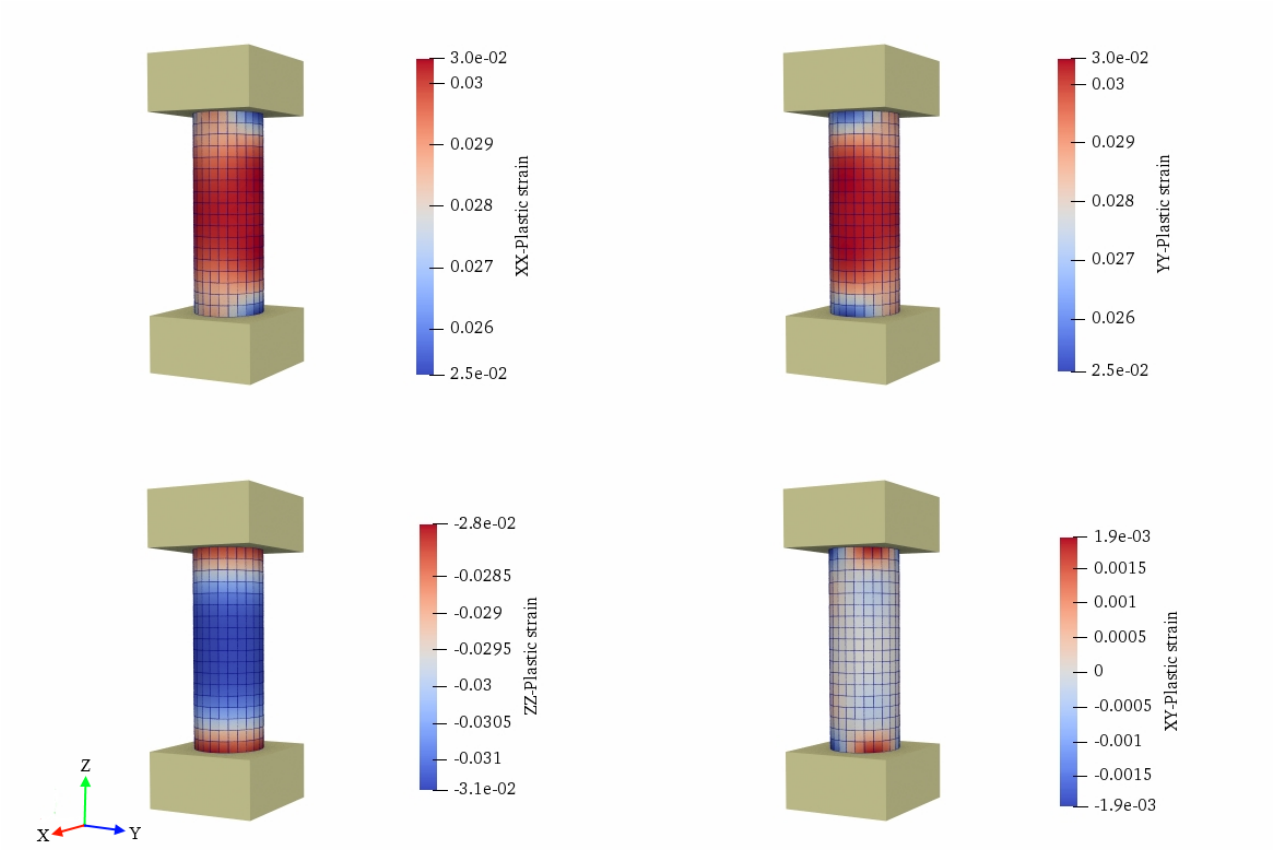

Figure 4.5: Distribution of plastic strains.

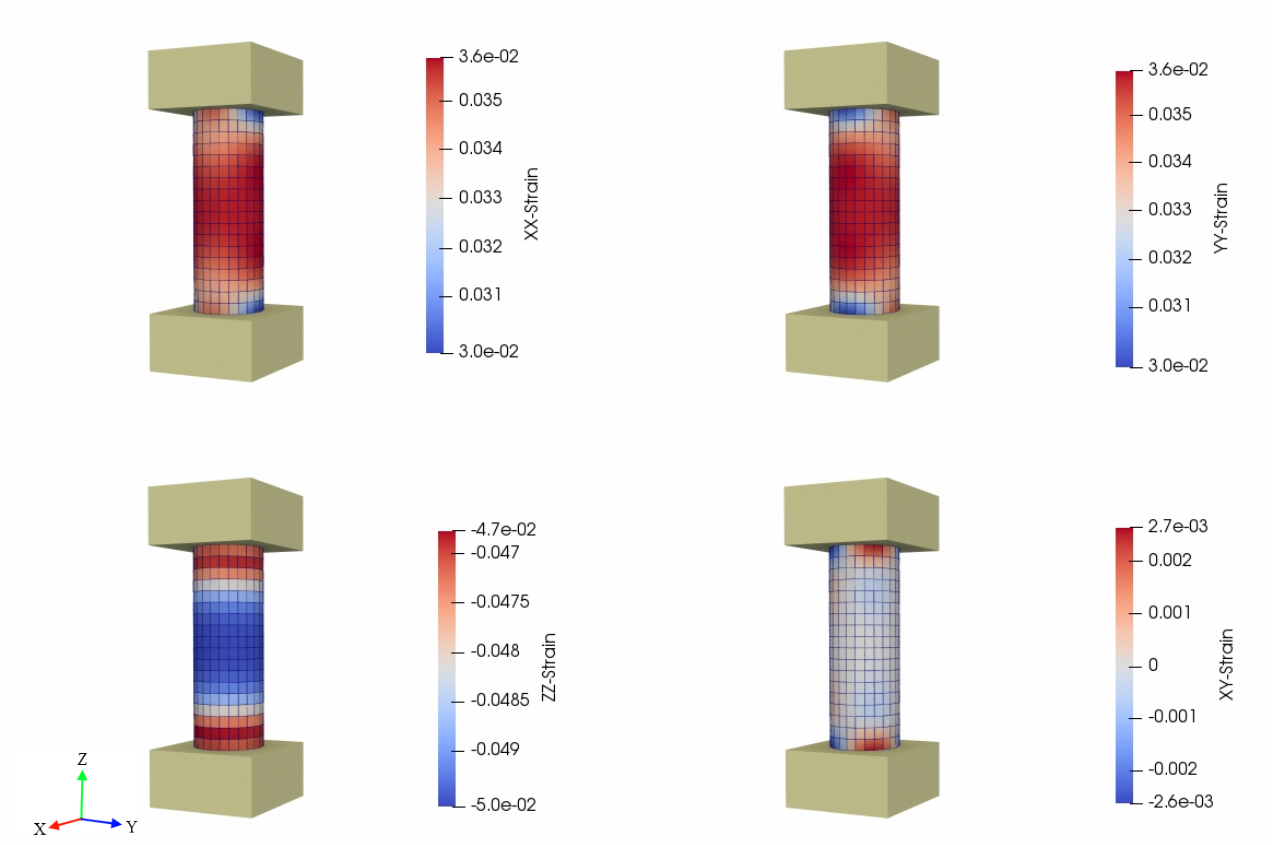

Figure 4.6: Distribution of total strains.

4.2 Testing of curing model

To verify the curing model already implemented in MARS solver, the experiment presented in [8] is utilized. More specifically, the temperature and degree of cure development in a pure epoxy cube is considered. The cube size equal to 4 mm is chosen. The temperature on the entire boundary is prescribed. The epoxy is completely uncured at 295 K (22°C) at time $t = 0$. The temperature is ramped up linearly within 100 s to 323 K (50°C). It is held at that level subsequently for 3600 s. The boundary temperature is then reduced to room temperature within 100 s. The material properties of the epoxy are: $\rho = 1200$ kg/m^3; $H_r = 227$ J/g; $A_1 = 3.62e11$ 1/s; $A_2 = 0.01$/s; $\Delta E_1 = 88.54$ kJ; $\Delta E_2 = 0.0$ kJ; $m = 0$; $n = 1$; $c = 200$ J/kgK; $\kappa = 0.2$ W/mK. The distribution of temperature and curing degree for time t=200 s is shown in Fig. 4.7. As can be seen, the highest temperature and thus the curing degree is experienced in the center of the cube. These results correspond to the data presented in [8] since the temperature is not uniform. During the time at which the boundary temperature is ramped up, the inside temperature lags the outside temperature. Moreover, the evolution of the temperature in the center with respect to time is plotted in Fig. 4.8., as well as the evolution of curing degree for the center point is shown in Fig. 4.9. Fig. 4.9 demonstrates deceleration of curing if with higher degree of cure is achieved.

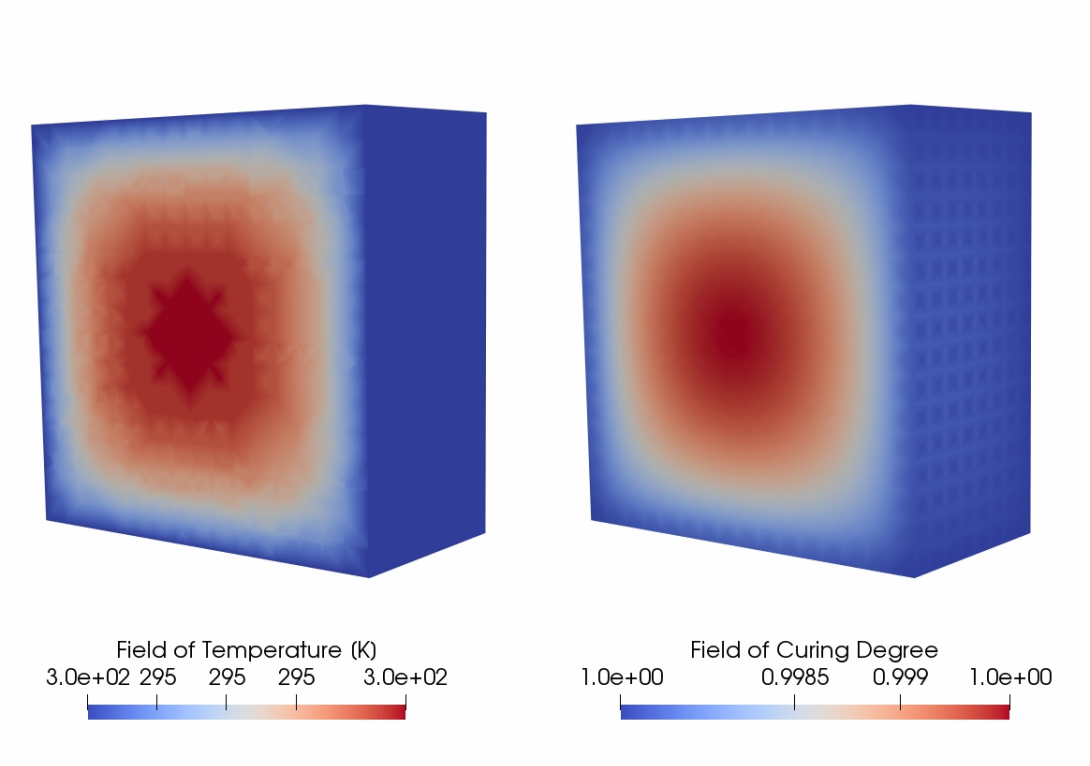

Figure 4.7: Epoxy cube at time $t = 200$ s (center slice): a) temperature; b) curing degree.

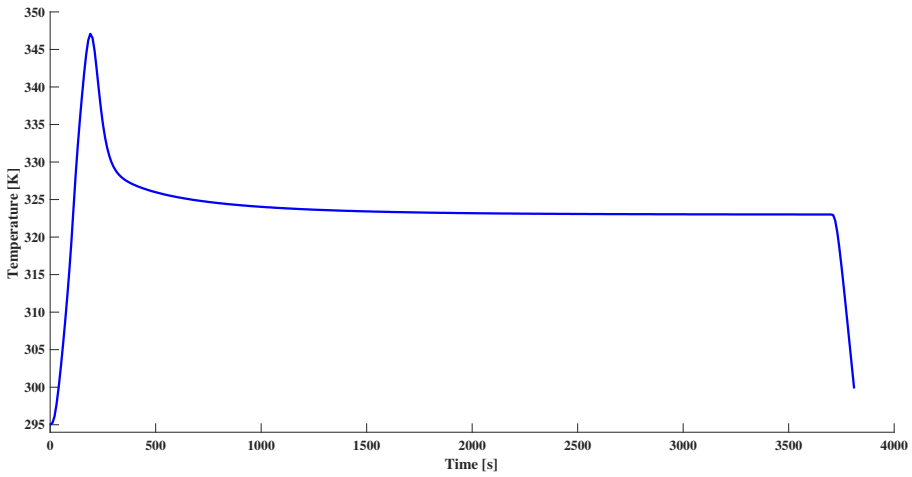

Figure 4.8: Temperature evolution in the cube center.

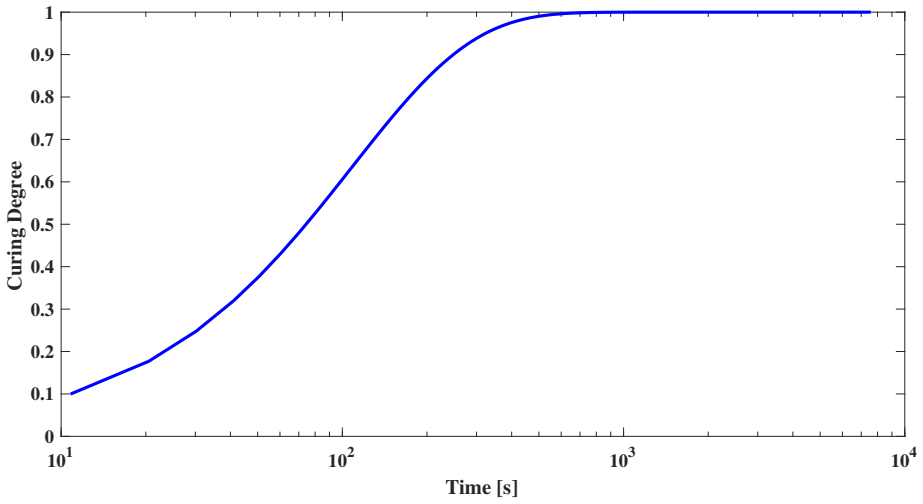

Figure 4.9: Degree of cure with respect to logarithmic time.

Conclusion and future work

The main aim of this work was to create a numerical model that describes sufficiently precisely the evolution of material properties and the behavior of thermoset polymers during the mechanical loading. In the first chapter, the different types of anchors are described and the divisions based on the installation time and the load transfer mechanism are presented. Finally, the failure modes of anchors are briefly summarized. The thermosetting polymers and their types are characterized in Chapter 2. The utilized numerical models together with the implementation procedure are described in Chapter 3. First the Drucker-Prager model is studied and its implementation into the FE software is presented. Then the curing model for polymers is briefly described and the evolution of material parameters is based on the curing degree. The idea of serially coupled models is also defined in Chapter 3. Finally, the results supporting the use of studied models are presented in Chapter 4. It should be noted that only preliminary results showing the capability of individual models are presented and more complex study is needed to really verify the aforementioned models. Moreover, some extensions of the models as suggested in [9] and presented results may be needed.

In general, the development of complex material model is a crutial step towards the successful modelling of bonded anchors. The presented work is the first attempt to fulfill this goal. As shown, the standard Drucker-Prager model may need some additional improvements and therefore the utilization of microplane material model [10] is expected in the future. The free volume approach presented in [11] will be also employed to simulate the time, temperature and humidity influence. These additional improvements and extensions are expected to be a part of the Master's thesis.

References

[1] ACI, "Building code requirements for structural concrete," Tech. Rep. 318M-08, ACI, 2008.

[2] Hilti, *Anchor Fastening Technology Manual*, 2012.

[3] S. S. Sakla and A. F. Ashour, "Prediction of tensile capacity of single adhesive anchors using neural networks," *Computers & Structures*, vol. 83, no. 21, pp. 1792 – 1803, 2005.

[4] J.-P. Pascault, H. Sautereau, J. Verdu, and R. J. Williams, *Thermosetting polymers*, vol. 64. CRC Press, 2002.

[5] M. Sejnoha, *GEO FEM - Theoretical manual*. FINE Ltd., 2009.

[6] ES3, "Mars - modeling and analysis of the response structures."

[7] G. Dhatt, E. LefranÃ, G. Touzot, *et al.*, *Finite element method*. John Wiley & Sons, 2012.

[8] C. Heinrich, M. Aldridge, A. S. Wineman, J. Kieffer, A. M. Waas, and K. W. Shahwan, "Generation of heat and stress during the cure of polymers used in fiber composites," *International Journal of Engineering Science*, vol. 53, pp. 85–111, 2012.

[9] R. Unterweger, *Experimentelle und numerische Untersuchungen zum Tragverhalten von chemischen Verankerungen*. PhD thesis, University of Natural Resources and Life Sciences, Vienna, 1999.

[10] G. Di Luzio, "A symmetric over-nonlocal microplane model m4 for fracture in concrete," *International journal of solids and structures*, vol. 44, no. 13, pp. 4418–4441, 2007.

[11] C. F. Popelar and K. Liechti, "Multiaxial nonlinear viscoelastic characterization and modeling of a structural adhesive," *Journal of Engineering Materials and Technology*, vol. 119, no. 3, pp. 205–210, 1997.